

This article was published in Applied Catalysis A: General, 470C, 45-55, 2014
<http://dx.doi.org/10.1016/j.apcata.2013.10.034>

**Effect of the preparation method on the catalytic activity and stability
of Au/Fe₂O₃ catalysts in the low-temperature water-gas shift reaction**

M. A. Soria¹, P. Pérez¹, S.A.C. Carabineiro², F. J. Maldonado-Hódar³, A. Mendes¹, Luis
M. Madeira^{1*}

¹ *LEPAE – Chemical Engineering Department, Faculty of Engineering - University of
Porto, Rua Dr. Roberto Frias, s/n, 4200-465 Porto, Portugal.*

² *LCM - Laboratory of Catalysis and Materials - Associate Laboratory LSRE/LCM,
Chemical Engineering Department, Faculty of Engineering - University of Porto, Rua
Dr. Roberto Frias, s/n, 4200-465 Porto Portugal.*

³ *Carbon Research Group - Inorganic Chemistry Department - Faculty of Sciences -
University of Granada, Spain.*

* Corresponding author. Tel.: +351-22-5081519; Fax: +351-22-5081449; E-mail:

mmadeira@fe.up.pt

Abstract

The low temperature water–gas-shift reaction has been studied over a series of nanosized Au/Fe₂O₃ catalysts. The effect of the synthesis method on the catalytic activity has been analysed. A series of catalysts with different Au loadings has been prepared by different methods: Deposition-Precipitation (DP), Liquid Phase Reductive Deposition (LPRD) and Double Impregnation Method (DIM). The Au/Fe₂O₃ catalysts prepared by DP showed the highest CO conversion. The catalysts were characterised by hydrogen temperature programmed reduction (TPR-H₂), high-resolution transmission electron microscopy (HRTEM), X-ray powder diffraction and X-ray photoelectron spectroscopy. TPR-H₂ analysis revealed that gold promotes the reducibility of the Fe₂O₃ support, which is crucial in this redox reaction. HRTEM evidences a very good dispersion of gold over the iron support, with nanoparticles in the range 2.2-3.1 nm for the DP and LPRD series, and a negligible increase in the average particle size of the used samples. For the DIM series, much larger Au particles (~6.6 nm) were obtained.

Keywords

Low temperature, Water-gas shift, Hydrogen, Au catalyst, Fe₂O₃, TPR, XRD, HRTEM.

1. Introduction

The water–gas shift (WGS) reaction (eq.1) is widely used in the chemical industry to convert CO from syngas into CO₂ and produce additional H₂ [1].



This is an important process to produce CO-free hydrogen or to adjust the H₂/CO ratio. The latter is especially desirable for downstream processes, such as Fischer-Tropsch and methanol synthesis [2]. On the other hand, high purity hydrogen is very important to use in fuel-cell power systems and ammonia synthesis, since CO is a poison for the iron catalyst used in ammonia production and for the anodic platinum electrode of the fuel cells [3, 4].

The WGS has the advantage that is a mildly exothermic equilibrium-limited reaction, thus is thermodynamically favoured at lower temperatures but it has the disadvantage that the reaction kinetics is reduced under such conditions, decreasing so the yield of H₂ and increasing the amount of catalyst required to reach valuable CO conversions. Traditionally, in order to achieve high reaction rate and a high CO conversion, the WGS reaction is carried out in two catalytic reaction steps including high-temperature shift (HT-WGS) and low-temperature shift (LT-WGS) reactors [1, 5]. The first step, HT-WGS, operates in the temperature range of 350–450 °C, which has fast reaction rate but low CO equilibrium conversion values. The second stage, LT-WGS, generally performed in the range of 200–250 °C, is thermodynamically favourable to further convert CO, but relatively slow in terms of reaction rate [6-10].

There are two main classes of materials used in industry for the WGS reaction: Fe–Cr oxide mixtures for HT-WGS and Cu–Zn or Co–Mo oxides for LT-WGS [1, 11]. It is also

known that oxide-supported noble metals (Pt, Au, etc.) are also able to catalyse the LT-WGS reaction [12-18], for which better catalysts are required.

In spite of their high cost, noble metal catalysts have been gaining increased interest in the last decades, due to their promising usage in fuel cell applications [11, 19]. Basically, *in situ* fuel cell grade production of hydrogen requires a WGS reactor loaded with catalysts that: (i) are non-pyrophoric, (ii) do not require pre-reduction treatment, and (iii) are robust in cycles of rapid heating and cooling. Cu-based conventional catalysts require strict reduction conditions that, after activation, are highly reactive towards air (pyrophoric), being hazardous during start-up and shut-down cyclic operation [20-22]. Au-based catalysts can be successfully used in those applications because they are able to overcome these drawbacks.

Different oxides (i.e. Fe₂O₃, TiO₂, ZnO, Zr₂O, CeO₂) have been described as supports for gold-based catalysts [14-18, 23-25]. The increase in activity when gold is added to these oxides in LT-WGS was explained as a synergetic effect between gold and the metal oxide [24-26]. The nature of the support plays an important role in the activity of Au-based catalysts. Particularly, in the case of Fe₂O₃ support, the Fe²⁺ / Fe³⁺ redox couple has a significant role in the WGS because the reaction takes place via a redox mechanism [25, 27, 28].

Deposition-precipitation (DP) and co-precipitation (CP) are the most common methods used for the synthesis of Au-based catalysts for LT-WGS reaction [20, 24, 25, 29-31]. Recently, liquid-phase reductive deposition (LPRD) and double impregnation (DIM) techniques have been also used to prepare these catalysts [32, 33]. These not so common and relatively new methods are environmentally and economically more favourable for the production of highly active Au-based catalysts. Moreover, Au-based catalysts

prepared by LPRD and DIM have shown good performances towards the CO oxidation reaction [33-36]. To the best of our knowledge, Au-based catalysts prepared by LPRD or DIM techniques have not been used for WGS reaction yet.

The aims of this work are: (i) to study how the preparation method and the amount of Au affect the activity of Au-based samples for the LT-WGS reaction, and (ii) to gain insight into the physico-chemical properties influencing the activity and stability of Au/Fe₂O₃ catalysts for the mentioned reaction.

2. Experimental

2.1 Catalysts Preparation

2.1.1 Double Impregnation Method (DIM)

The DIM method is similar to the traditional wetness impregnation, but it involves a second impregnation step with the addition of an aqueous solution of Na₂CO₃ [33, 37, 38]. First, the support was impregnated with an aqueous solution (5×10^{-3} M) of H₂AuCl₄·3H₂O (Alfa Aesar) and then with an aqueous solution of Na₂CO₃ (10^{-2} M), under constant ultrasonic stirring. The slurry was then thoroughly washed with distilled water and dried in an oven at 120 °C overnight. α -Fe₂O₃ (Sigma Aldrich) was used as support. Different amounts of Au (1.5, 3 and 5 wt. %) were used, thus providing samples with different metal loads. The experimental content of gold in similar samples prepared by DIM was checked by means of ICP and was reported in several previous works [34, 39-41].

2.1.2 Liquid Phase Reductive Deposition (LPRD)

An aqueous solution of H₂AuCl₄·3H₂O (5×10^{-3} M) was mixed with an aqueous solution (2×10^{-2} M) of NaOH (1:4 weight ratio) with stirring at room temperature [32, 36, 42, 43].

The resulting solution was aged in the dark, at room temperature, for 24 h, in order to complete the hydroxylation of Au^{3+} ions. Then, the appropriate amount of support ($\alpha\text{-Fe}_2\text{O}_3$) was added to the solution and, after ultrasonic dispersion for 30 min, the suspension was aged in the oven, at 100 °C, overnight. The resulting solid was washed repeatedly with distilled water for chloride removal and again dried in the oven at 100 °C overnight. Different Au-based catalysts with 1.5, 3 and 5 wt. % of Au were prepared. The actual gold loading for samples prepared by LPRD was assessed by ICP as reported in several previous works [41, 43].

2.1.3 Deposition-precipitation (DP)

Several samples containing 1.5, 3 and 5 wt. % of Au were prepared by the DP method [44]. A solution of NaOH (1 M) was added to an aqueous solution of HAuCl_4 (5×10^{-3} M) in order to rise the pH of the solution to 9. The support ($\alpha\text{-Fe}_2\text{O}_3$) was then added with stirring at room temperature (1 g per 50 ml of solution). The resulting suspension was heated to 70 °C and vigorously stirred for 1 h; after cooling the solid obtained was filtered, thoroughly washed with deionized water and then vacuum-dried at room temperature.

In all the methods reported above, a commercial $\alpha\text{-Fe}_2\text{O}_3$, with a BET surface area of $6 \text{ m}^2 \text{ g}^{-1}$ and an average particle size of 63 nm [38], was used as support. The catalysts prepared by DP, LPRD and DIM techniques were labelled as $x\text{Au/Fe}_2\text{O}_3\text{_{DP}}$, $x\text{Au/Fe}_2\text{O}_3\text{_{LPRDP}}$ and $x\text{Au/Fe}_2\text{O}_3\text{_{DIM}}$, respectively, where x represents the nominal loading of Au in wt. %. For the DP series, the actual gold loading was 1.6 ± 0.1 , 2.5 ± 0.1 and 4.6 ± 0.2 wt. % for samples $1.5\text{Au/Fe}_2\text{O}_3\text{_{DP}}$, $3\text{Au/Fe}_2\text{O}_3\text{_{DP}}$ and $5\text{Au/Fe}_2\text{O}_3\text{_{DP}}$, respectively, as determined by absorption atomic spectroscopy (AAS – cf. section 2.3).

The Au/Fe₂O₃ (5 nominal wt. % of Au) catalyst, supplied by the World Gold Council (WGC), was also used for comparison purposes. This catalyst was labelled as 5Au/Fe₂O₃_reference and contains 4.7 ± 0.2 wt. % of Au as determined by AAS.

2.2 Catalytic Activity Runs

Activity measurements were carried out in a fixed-bed reactor. This reactor consists in a stainless steel tube with a length of 60 mm and 10 mm o.d., loaded with 0.2 g of Au-based catalyst ($\varnothing < 200 \mu\text{m}$) diluted with glass beads (Sigma Aldrich 212-300 μm) and framed in both ends by two discs of stainless steel mesh (10-15 μm).

Before WGS tests, the catalyst was heated in situ up to 200 °C (5 °C/min) under 50 ml_N/min N₂ flow. Then, the catalyst was reduced at this temperature using 50 ml_N/min of a 15% H₂/N₂ feed mixture. After 45 minutes of reduction, a 50 ml_N/min of N₂ flow was used during 30 min to sweep H₂ from the system. The catalyst was then exposed to a standard water–gas shift composition feed of 4.7 vol. % CO, 10.1 vol. % CO₂, 35.4 vol. % H₂O and 28.5 vol. % H₂, balanced with N₂. The catalytic tests were performed at atmospheric pressure, at different temperatures between 150 and 300 °C, with a total flow rate of 50 ml_N/min (thus the contact time was $W/Q = 6.67 \times 10^{-5} \text{ g}\cdot\text{h}\cdot\text{ml}_N^{-1}$).

Figure 1 shows the set-up used for the catalytic activity measurements in the LT-WGS reaction. The feed gases were controlled by mass flow controllers (Bronkhorst). A Controlled Evaporation and Mixing (CEM, Bronkhorst) unit was used to evaporate the water while mixing the generated steam with the feed gases. The reactor was encased in an electric oven (Mettler, Type UNE200), controlled by a programmable temperature controller. The tubes between the CEM and the reactor were heated at 115 °C in order to prevent steam condensation. Moisture in the product reaction gases was condensed by a peltier cooling placed at the reactor output (Marlow industries, model RC 12-6L).

The dry product gases were analysed with a DANI 1000 gas chromatograph equipped with a chromatographic column (Supelco Carboxen 1010 Plot, from Sigma-Aldrich, 30 m × 0.32 mm i.d.) and a micro-thermal conductivity detector (TCD) and operated with He as carrier gas (1 mL_N min⁻¹). The catalytic activity was expressed as percentage of the CO conversion (X_{CO} (%)) calculated as $[(F^{in} - F^{out}) / F^{in}] \times 100$, where F^{in} and F^{out} are the CO molar flow at the input and output of the reactor, respectively.

Thermodynamic equilibrium CO conversion (X_{COeq}) was calculated by means of the Gibbs free energy minimization method via ASPEN-HYSYS software, as described elsewhere [45].

2.3 Catalysts Characterisation

The gold loading was determined by atomic absorption spectrometry (AAS) by means of a Unicam 939 atomic absorption spectrophotometer equipped with a deuterium lamp background correction. An Au hollow cathode lamp (Heraeus), operating at 242.8 nm, was used as the radiation source. For the analysis, 20 mg of sample were diluted in aqua regia by agitation at room temperature. The error of the analysis was within ± 5 %.

Temperature programmed reduction (TPR-H₂) experiments were performed in a fully automated AMI-200 Catalyst Characterization Instrument (Altamira Instruments), equipped with a quadruple mass spectrometer (Dymaxion 200 amu, Ametek). In a typical TPR-H₂ experiment, 50 mg of sample was placed in a U-shaped quartz tube located inside an electrical furnace and subjected to a 10 °C/min heating rate up to 1000 °C, under He flow of 29 mL_N/min and H₂ flow of 1.5 mL_N /min.

High-resolution transmission electron microscopy (HRTEM) images were obtained by means of a Phillips CM-20 electron microscope which operated at 120 kV and with point-

to-point resolution of 2.7 Å and 0.14 Å between lines. The images were recorded at direct magnification of 600,000x and were used for the particle size and particle size distribution determination. For the analysis, the powders were dispersed in ethanol and homogenized by ultrasonic dispersion before “fishing” the catalysts particles from the dispersion, allowing the drying at ambient conditions.

X-ray diffraction (XRD) was carried out with a Bruker D8 Advance diffractometer using the $K\alpha$ radiation of Cu. The 2θ range between 10 and 80° was scanned with a step of 0.02° and step time of 15 s.

The X-ray photoelectron spectroscopy (XPS) analysis was performed using a Kratos AXIS Ultra HSA apparatus, with VISION software for data acquisition and CASAXPS software for data analysis (spectra deconvolution). The analysis was carried out with a monochromatic Al $K\alpha$ X-ray source (1486.7 eV), operating at 15 kV (90 W), in FAT mode (Fixed Analyser Transmission), with a pass energy of 40 eV for regions ROI and 80 eV for survey. The binding energies were calibrated by fixing the C-(C, H) contribution of the C1s adventitious carbon at 285 eV. Data acquisition was performed with a pressure lower than 1×10^{-6} Pa, and it was used a charge neutralisation system.

3. Results

3.1 Catalytic activity

Figure 2 shows CO conversion (X_{CO}) as a function of temperature for the LT-WGS reaction for the different Au/Fe₂O₃ catalysts prepared by the DP method; it also includes data gathered with the 5Au/Fe₂O₃ _reference catalyst from World Gold Council. The equilibrium CO conversion is also included in this figure. Samples 5Au/Fe₂O₃_DP, 3Au/Fe₂O₃_DP and 5Au/Fe₂O₃_reference show a similar trend regarding the CO

conversion, namely, it increases from 150 to around 200 °C and then decreases for higher temperatures. In the case of 1.5Au/Fe₂O₃_DP sample, the X_{CO} steadily increases with reaction temperature, reaching a maximum at 250 °C. A further increase of temperature results in a slight decrease of X_{CO} .

Whatever the temperature, the activity of the Au-based catalysts prepared by the DP technique increases with the Au loading (5Au/Fe₂O₃_DP > 3Au/Fe₂O₃_DP > 1.5Au/Fe₂O₃_DP). Furthermore, the 5Au/Fe₂O₃_DP catalyst is more active than the 5Au/Fe₂O₃_reference in the entire range of the temperatures explored. It is worth noting that at 300 °C the 3Au/Fe₂O₃_DP (3 wt.% Au) catalyst shows nearly the same activity as the commercial sample, despite the latter having a higher Au loading (5 wt.%).

CO conversion as a function of temperature for the Au-based catalysts prepared by LPRD method is shown in Figure 3. The activity of these catalysts is higher for smaller Au loadings (1.5Au/Fe₂O₃_LPRD > 3Au/Fe₂O₃_LPRD > 5 Au/Fe₂O₃_LPRD), showing the opposite trend as the counterpart catalysts prepared by DP. For all catalysts, the activity increases with temperature up to 250 °C; afterwards it remains nearly constant (1.5Au/Fe₂O₃_LPRD) or slightly decreases (3 and 5 wt. % Au).

The Au-based catalysts prepared by the DIM method have a very low CO conversion (\leq 10 %) in the range of temperatures analysed (data not shown).

With the more promising catalytic materials, DP series, further tests were then carried out. Namely, the stability of the 3Au/Fe₂O₃_DP catalyst was assessed based on the CO conversion history studied at 200 °C. The results obtained are shown in Figure 4. It can be seen that carbon monoxide conversion with such material decreases slowly during the first 20 h of reaction, and then tends to stabilize.

Figures 5a-5b illustrate the catalytic activity of the 5Au/Fe₂O₃_DP and a 3Au/Fe₂O₃_DP samples, respectively, as a function of temperature during: (i) an heating step (T is increased from 150 to 300 °C) and (ii) a cooling step (T is decreased from 300 to 150 °C). This figure clearly shows that regardless of temperature, the X_{CO} value recorded during the decreasing temperature test (300 °C → 150 °C) is always dramatically lower than the corresponding counterpart during the increasing temperature test (150 °C → 300 °C).

3.2 Characterisation

3.2.1 TPR-H₂

The TPR-H₂ results obtained for bulk α -Fe₂O₃, 5Au/Fe₂O₃_reference and Au/Fe₂O₃_DP samples are illustrated in Figure 6. Large differences in the reducibility of the bulk α -Fe₂O₃ and the Au/Fe₂O₃_DP samples can be seen. Bulk α -Fe₂O₃ presents a very sharp peak centred at 390 °C and two partially overlapped broad peaks with maxima at ~650 and ~900 °C, respectively. The Au/Fe₂O₃_DP catalysts present a sharp peak at low temperature (~265 °C) and another broad peak at higher temperature (~565 °C). It should be noted that, in the case of 1.5Au/Fe₂O₃_DP, both peaks are shifted towards slightly higher temperatures, compared to the catalysts with higher Au loading (3 and 5 wt.% Au). Furthermore, the high temperature peak is broader than those of the other samples and presents a shoulder around 700 °C.

The TPR-H₂ profiles for the series of samples prepared by the DIM technique are shown in Figure 7. The samples containing 1.5 and 3 wt. % of Au exhibit four major peaks at ~180, ~360, ~570 and ~770 °C. The 5Au/Fe₂O₃_DIM sample shows a very similar TPR-H₂ profile; the only difference is that the peak at the lower temperature appears at 300 °C instead of 180 °C.

TPR-H₂ profiles for the samples prepared by LPRD are given in Figure 8. All the samples show two small peaks at ~150 and ~270 °C and two large overlapped peaks between ~400 and ~850 °C.

3.2.2 XRD

Figures 9 and 10 show the X-ray diffraction patterns of some fresh and used Au-based samples that revealed to be particularly active; samples used refer to those employed in runs at 300 °C, unless otherwise stated. Fresh catalysts 5Au/Fe₂O₃_DP, 1.5Au/Fe₂O₃_LPRD (Figure 9) and 3Au/Fe₂O₃_DP (Figure 10) present the same diffraction patterns with peaks at 24.1°, 33.1°, 35.6°, 40.9°, 49.5°, 54.2°, 57.6°, 62.5°, 64.1°, 72.0° and 75.6°, characteristic of the crystal structure of rhombohedral hematite α -Fe₂O₃ (JCPDS file N° 86-0550). The XRD patterns of the used samples are clearly different. The spent 5Au/Fe₂O₃_DP sample (Figure 9, diffractogram d) shows reflections at 18.4°, 30.1°, 35.4°, 37.1°, 43.2°, 53.6°, 57.1°, 62.6°, 71.2°, 74.0° and 75.0° which match with cubic magnetite reference (Fe₃O₄; JCPDS file N° 80-0390). The diffractogram d also presents a broad peak at 38.2° corresponding to Au⁰ (JCPDS file N° 04-0784). The spent 1.5Au/Fe₂O₃_LPRD catalyst (Figure 9, diffractogram b) shows reflections attributed to magnetite, and other peaks assigned to siderite (FeCO₃; JPCDS file N° 83-1764) and Au⁰. The spent 3Au/Fe₂O₃_DP catalyst (Figure 10, diffractogram b), besides hematite, magnetite and Au⁰ also exhibit peaks assigned to siderite, while the 3Au/Fe₂O₃_DP sample after stability test at 200 °C for 25 h (Figure 10, diffractogram c) just shows peaks attributed to hematite and magnetite. Au₂O or Au₂O₃ were not observed in any of the XRD patterns.

3.2.3 HRTEM

Figures 11a-11d give representative HRTEM images of the fresh and used Au-based catalysts prepared by DP and LPRD techniques that revealed to be more active. Au nanoparticles (indicated by an arrow in the figure) can be clearly distinguished from the Fe₂O₃ support. The gold cores look distinctly darker than the iron oxide due to the higher electron density. The HRTEM images clearly demonstrate that the Au nanoparticles are homogeneously distributed over the support on the catalyst before and after reaction.

The Au particle size distributions of some fresh and used catalysts are shown in Figures 12 and 13, respectively. HRTEM analysis for Au-based catalysts prepared by DP and DIM methods reveals that the average gold nanoparticle size is very similar regardless the gold loading (~2.3 and 6.6 nm for DP and DIM respectively). However, for Au/Fe₂O₃_LPRD catalysts the average gold nanoparticle size slightly increases with the loading of Au (2.5 and 3.1 nm for 1.5 and 5 wt. % Au, respectively). For the series of Au/Fe₂O₃ used samples, the gold (average) nanoparticle size increased very little after reaction.

3.2.4. XPS

Figure 14 compares the XPS Au 4f spectra for the as-prepared 5Au/Fe₂O₃_DIM, 3Au/Fe₂O₃_DP and 1.5Au/Fe₂O₃_LPRD catalysts. In all the Au-based samples the Au 4f XPS peak appears as a doublet; 4f_{7/2} and 4f_{5/2}.

According to the peaks position of the Au 4f_{7/2} and 4f_{5/2} and comparing with the literature [38, 46-49], it can be inferred that the sample prepared by the DP method has cationic gold (Au¹⁺ and Au³⁺), while the catalysts prepared by LPRD and DIM methods contain mainly metallic gold (Au⁰).

4. Discussion

4.1 Effect of gold on the reducibility of the α -Fe₂O₃ support

The TPR-H₂ profile of the support (Figure 6) indicates that α -Fe₂O₃ is reduced in a three-step mechanism. The low temperature peak was attributed to the first stage of reduction of hematite to magnetite (Fe₂O₃ → Fe₃O₄) [27, 50, 51]. The two high temperature peaks were assigned to the two-step magnetite reduction sequence, namely: Fe₃O₄ → FeO → Fe [27, 50, 51]. This three-step mechanism of α -Fe₂O₃ reduction is consistent with several results reported in literature [27, 31, 51-53]. However, other authors claimed that the reduction of α -Fe₂O₃ proceeds by a two-step mechanism (Fe₂O₃ → Fe₃O₄ → Fe), based on the fact that only two peaks were observed [50, 51, 54]. The peak at low temperature is attributed to reduction of hematite into magnetite (Fe₂O₃ → Fe₃O₄) and the high temperature peak is assigned to direct reduction of Fe₃O₄ into Fe. This difference of reduction mechanism depends on the operational condition used for TPR experiment (i.e. mass/type of the catalyst, heating rate, composition of H₂ stream, etc.).

As evidenced by XRD, in the as-synthesized Au/Fe₂O₃_DP catalysts (Figures 9-10), only one phase is present, corresponding to Fe₂O₃. Therefore, the peak at low temperature in the TPR-H₂ profile could be ascribed to the reduction of Fe₂O₃ into Fe₃O₄. It is important to note that the higher the Au loading in the DP series, the higher is the shift of this peak towards lower temperatures with respect to that of the Fe₂O₃ support (Figure 6). This trend is in agreement with previous studies of Au/Fe₂O₃ catalysts reported in literature [23, 27, 55, 56] where this effect was explained in terms of the activation (adsorption-dissociation) of molecular hydrogen on the gold metal and the spillover of the atomic hydrogen to the α -Fe₂O₃ material [23, 27, 57, 58], and is supported by the fact that the Au-particle size is independent of the metal loading (Figure 12).

As already mentioned, the high temperature peaks attributed to successive reduction of Fe_3O_4 in $\text{Au}/\text{Fe}_2\text{O}_3$ _DP samples is different from that of the $\alpha\text{-Fe}_2\text{O}_3$ support. In fact, these catalysts show only one broad peak that is shifted (~ 100 °C) to lower temperatures compared with the $\alpha\text{-Fe}_2\text{O}_3$ profile. This shows that the presence of Au not only promotes the reduction of Fe_3O_4 , but changes the reduction mechanism of Fe_3O_4 from a two-step process ($\alpha\text{-Fe}_2\text{O}_3$, two overlapped peaks) to a one-step process ($\text{Au}/\text{Fe}_2\text{O}_3$ one single peak).

The TPR- H_2 profiles of the Au-based samples prepared by DIM (Figure 7) and LPRD (Figure 8) methods point to the same conclusion as in the DP catalysts, namely, gold promotes the reducibility of the $\alpha\text{-Fe}_2\text{O}_3$ support. However, for these samples, the reduction of Fe_3O_4 to metallic Fe occurs in a two-step process, similarly to the $\alpha\text{-Fe}_2\text{O}_3$ support. It is clear that the reducibility of the Au-based catalysts is strongly different depending on the synthesis method. Indeed, according to the preparation, the Fe_2O_3 reducibility decreases in the order: DP > LPRD > DIM. This suggests a higher interaction between the gold and the Fe_3O_2 in the DP method, which resulted in more active catalysts.

There is not a general consensus in the literature about the temperature at which supported gold oxide is reduced. The reduction of bulk gold oxide was reported as two sharp reduction peaks at 195 °C and at 232 °C [53]. Some authors observed the reduction of gold oxide in the 100-150 °C range for $\text{Au}/\text{Fe}_2\text{O}_3$ samples prepared by the co-precipitation method [48, 58, 59]. They claimed that the peak of reduction of Au_xO_y species appears at lower temperature, with respect to bulk gold oxide, as a consequence of a much higher surface area of $\text{Au}/\text{Fe}_2\text{O}_3$ catalysts [48, 60].

Nevertheless, other authors reported that the reduction of the Au_xO_y species occurs at higher temperature (224 °C) in Au-based samples [48, 52, 53] prepared by the DP

technique. In this case, it is assumed that the reduction of gold oxides and Fe_2O_3 to Fe_3O_4 transformation occurs simultaneously. It was argued that some sort of interaction between the iron oxide and the Au species could explain why the reduction of gold species occurs at higher temperature. This latter issue is in good agreement with our finding for the Au-based samples prepared by the DP method (Figure 6), suggesting a strong interaction between Au and Fe.

On the other hand, XPS of the samples prepared by DP method shows the presence of gold as Au^{1+} and Au^{3+} (Figure 14), although no crystalline Au_xO_y species were found by XRD, even in the sample containing 5 wt. % of Au. It seems likely that such species are highly dispersed as evidenced by HRTEM. In addition, based on the fact that the area of the lower temperature peak increases as a function of the loading of Au (cf. Figure 6), it appears that the reduction of both gold and iron oxides occurs simultaneously in Au/ Fe_2O_3 _DP samples.

As for the Au-based samples prepared by DIM and LPRD methods, XPS analysis reveals that these catalysts contain principally metallic gold. Therefore, it is very likely that the broad peak observed at around 150 °C in the TPR- H_2 corresponds to the reduction of the hydroxylated iron oxide. Besides, for this kind of samples it was reported that the reduction of the hydroxylated iron oxide occurs at this temperature [38].

4.2 Influence of the preparation method over the catalyst's activity in the LT-WGS reaction

As already said, the Au/ Fe_2O_3 _DP and 1.5Au/ Fe_2O_3 _LPRD catalysts were very active in the LT-WGS reaction. This confirms what was found in previous works [24, 25, 28, 61, 62] for samples prepared by DP or co-precipitation methods. Moreover, it was found that the CO conversion increases with the temperature, reaching a maximum (around 200-250

°C) and then slightly decreases with further temperature increase. A similar trend was already reported elsewhere [24, 25, 28, 61, 62].

The CO conversion of Au/Fe₂O₃ catalysts prepared by the DP and DIM methods changes according to the following trend: 5Au/Fe₂O₃ > 3Au/Fe₂O₃ > 1.5Au/Fe₂O₃. The fresh 5Au/Fe₂O₃ (Au average particle size = 2.2 nm), 3Au/Fe₂O₃ (Au average particle size = 2.5 nm) and 1.5Au/Fe₂O₃ (Au average particle size = 2.3 nm) samples prepared by DP show nearly the same Au average particle size, as evidenced by HRTEM (Figure 12). This suggests that Au is highly dispersed over the samples, although they have different Au contents. In the case of the Au/Fe₂O₃ catalysts prepared by DIM method, the Au average particle size is 6.6 nm for 1.5Au/Fe₂O₃_DIM and 5Au/Fe₂O₃_DIM fresh samples. Thus, for Au/Fe₂O₃_DP (and also Au/Fe₂O₃_DIM) catalysts, the activity strongly depends on the Au loading, increasing for higher metal loads because its dispersion is nearly not affected.

However, for the catalysts prepared by the LPRD method the activity follows the opposite trend, namely: 1.5Au/Fe₂O₃_LPRD > 3Au/Fe₂O₃_LPRD > 5Au/Fe₂O₃_LPRD. HRTEM analysis of 1.5Au/Fe₂O₃_LPRD and 5Au/Fe₂O₃_LPRD fresh catalyst reveals that the Au average particle size is 2.5 and 3.1 nm, respectively. This suggests that the activity of the Au/Fe₂O₃_LPRD catalysts depends on the Au nanoparticles dispersion.

Comparing the activity of the catalysts prepared by the different techniques, X_{CO} decreases according to the following order: Au/Fe₂O₃_DP > Au/Fe₂O₃_LPRD > Au/Fe₂O₃_DIM. This trend matches the order of interaction between the gold and the Fe₂O₃ as suggested by TPR analysis; the strongest is the metal-support interaction, the highest is the activity. Therefore, this indicates that the high catalytic activity of the Au/Fe₂O₃ catalysts is not only related to the gold dispersion but also to a higher interaction

of gold particles with the iron oxide support, both these issues depending on the adopted preparation method.

On the other hand, the slightly decrease of activity observed in Au/Fe₂O₃_DP and Au/Fe₂O₃_LPRD samples above 200-250 °C (cf. Figures 2 and 3, respectively) could be related to the sintering of gold particles. However, HRTEM of some of the used catalysts prepared by DP and LPRD did not show significant changes in Au particle size. Thus, it seems that sintering of Au particles per se cannot account for the loss of activity shown by Au/Fe₂O₃_DP and Au/Fe₂O₃_LPRD samples, but other aspects must be also taken into account, such as changes of the oxidation state of iron, as observed by XRD (Figure 9 and 10).

Some authors [25, 27, 28] reported that the formation of CO₂ and H₂ in WGS reaction occurs via a reduction-oxidation mechanism of the α -Fe₂O₃. The XRD patterns of some used catalysts evidence changes of the iron oxide phase, which depends on the preparation method and for the same method on the Au content (Figures 9-10). For example, in the used 5Au/Fe₂O₃_DP only magnetite (Fe₃O₄) is observed, while in the spent 3Au/Fe₂O₃_DP sample residual hematite (Fe₂O₃), magnetite and siderite (FeCO₃) are observed, and in the used 1.5Au/Fe₂O₃_LPRD magnetite and siderite are seen. This clearly indicates that changes of the iron oxide structure take place during reaction, in good agreement with TPR results, which shows that reduction of ferrite to magnetite occurs around 200 °C. Thus, a suitable ratio between both oxidation states, i.e. Fe²⁺ and Fe³⁺ species, seems essential for high catalytic activity.

4.3 Stability of the catalysts

Carbon monoxide conversion with the time on stream on 3Au/Fe₃O₂_DP catalyst showed a loss of activity during the first 20 h of reaction (Figure 4). Indeed, catalytic deactivation

has also been observed during cyclic temperature-programed operation (Figure 5) since in the cooling stage (300 to 150 °C) CO conversion does not reach the values obtained during the heating stage (150 to 300 °C). Deactivation of the Au/Fe₂O₃ catalysts has also been reported elsewhere [28]. The HRTEM of the 3Au/Fe₃O₂_DP sample after stability test shows that the average gold nanoparticle size (Figure 13d) did not vary with respect to the fresh sample (Figure 12b). Therefore, apparently no sintering occurred during the stability test. According to the study of reducibility of the Au/Fe₂O₃_DP catalysts and their characterization (HRTEM and XRD) after reaction, it seems likely that the stability of the catalyst mainly depends on the oxidation state of the iron species during reaction.

4.4 Performance of the materials vs. other catalysts

Figure 15 compares the carbon monoxide conversion at different reaction temperatures for the 5Au/Fe₂O₃_DP catalyst (material prepared in this work exhibiting the highest X_{CO} values) and Au/Fe₂O₃ catalysts reported in the literature. Table 1 summarizes the gold content, specific surface area (S_{BET}) of this series of catalysts, as well as the experimental conditions used for the tests. A proper comparison between our results and those reported in the literature is hard to establish due to the very different working conditions and/or catalysts employed, as shown in Table 1. Despite of the latter, the catalyst prepared in this work is among the best performing catalysts (Figure 15), even if in the reactor feed a reformat stream containing WGS products has been employed and the catalyst has been prepared from a support with a very low surface area.

5. Conclusions

The TPR-H₂ profiles of the Au/Fe₂O₃ system reveals that gold promotes the reducibility of the Fe₂O₃ support. The activity of the Au/Fe₂O₃ catalysts prepared by DP and LPRD is dependent of the Au loading, but they follow opposite trends. In fact, for the

Au/Fe₂O₃_DP samples, the highest activity in the LT-WGS reaction matches the highest Au content (5 wt. %), whereas for the Au/ Fe₂O₃_LPRD samples the catalyst containing the lowest nominal amount of Au (1.5 wt. %) was the most active. This was assigned to the higher Au nanoparticles size found on samples prepared by LPRD with higher loadings, thus affecting the gold dispersion over the support; for the DP series, Au dispersion was almost not affected (particle size ~2.3 nm). For the Au/Fe₂O₃_DIM catalysts, a much larger size of the Au nanoparticles was obtained (6.6 nm).

The catalytic activity of Au/Fe₂O₃ catalysts strongly depends not only on the dispersion of gold, but also on the reducibility of the support. Gold is highly dispersed on iron oxide, with Au average particle size in the range of 2.2-3.1 nm for DP and LPRD series. Regarding stability, 3Au/Fe₂O₃_DP catalyst became somewhat deactivated with time on stream, but this is mostly related to changes in iron oxidation state, not to Au sintering; after a period of ca. 20 h activity tended to stabilize.

Acknowledgements

The authors acknowledge financing from the Portuguese Foundation for Science and Technology (FCT) through the project PTDC/EQU-ERQ/098730/2008. M.A. Soria, Patricia Pérez and Sónia Carabineiro are grateful to the FCT for the postdoctoral grant (SFRH / BD / 88444 / 2012), doctoral grant (SFRH / BD / 73673 / 2010) and for the CIENCIA 2007 program, respectively.

5. References

- [1] Ke Liu, Chunshan Song, V. Subramani, Hydrogen and Syngas Production and Purification Technologies, Wiley, Alche, January 2010.
- [2] J. Li, H. Yoon, T.-K. Oh, E.D. Wachsman, Int J of Hydrogen Energ 37 (2012) 16006-16012.
- [3] D. Cameron, R. Holliday, D. Thompson, J Power Sources 118 (2003) 298-303.
- [4] H.F. Abbas, W.M.A. Wan Daud, Int J of Hydrogen Energ 35 (2010) 1160-1190.
- [5] D. Ma, C.R.F. Lund, Ind. Eng. Chem. Res 42 (2003) 711-717.
- [6] J.Y. Lee, D.-W. Lee, K.-Y. Lee, Y. Wang, Catal Today 146 (2009) 260-264.
- [7] M. Maroño, E. Ruiz, J.M. Sánchez, C. Martos, J. Dufour, A. Ruiz, Int J of Hydrogen Energ 34 (2009) 8921-8928.
- [8] T.A. Adams li, P.I. Barton, Int J of Hydrogen Energ 34 (2009) 8877-8891.
- [9] P. Gawade, B. Mirkelamoglu, U.S. Ozkan, J. Phys. Chem. C 114 (2010) 18173-18181.
- [10] D. Mendes, A. Mendes, L.M. Madeira, A. Iulianelli, J.M. Sousa, A. Basile, Asia-Pac. J. Chem. Eng 5 (2010) 111-137.
- [11] C. Ratnasamy, J.P. Wagner, Catal Rev 51 (2009) 325-440.
- [12] Q. Fu, H. Saltsburg, M. Flytzani-Stephanopoulos, Science 301 (2003) 935-938.
- [13] T. Bunluesin, R.J. Gorte, G.W. Graham, Appl Catal B-Environ 15 (1998) 107-114.
- [14] C.H. Kim, L.T. Thompson, J Catal 230 (2005) 66-74.
- [15] B.A. Lenite, C. Galletti, S. Specchia, Int J of Hydrogen Energ 36 (2011) 7750-7758.
- [16] V. Idakiev, T. Tabakova, Z.Y. Yuan, B.L. Su, Appl Catal A-Gen 270 (2004) 135-141.
- [17] Y. Zhang, Y. Zhan, C. Chen, Y. Cao, X. Lin, Q. Zheng, Int J of Hydrogen Energ 37 (2012) 12292-12300.
- [18] D. Mendes, H. Garcia, V.B. Silva, A.I. Mendes, L.M. Madeira, Ind Eng Chem Res 48 (2008) 430-439.
- [19] D.L. Trimm, Appl Catal A-Gen 296 (2005) 1-11.
- [20] D. Andreeva, I. Ivanov, L. Ilieva, M.V. Abrashev, App Catal A-Gen 302 (2006) 127-132.
- [21] A. Faur Ghenciu, Current Opinion in Solid State and Materials Science 6 (2002) 389-399.
- [22] S. Hilaire, X. Wang, T. Luo, R.J. Gorte, J. Wagner, App Catal A-Gen 258 (2004) 271-276.
- [23] D. Andreeva, Gold Bull 35 (2002) 82-88.
- [24] D. Andreeva, V. Idakiev, T. Tabakova, A. Andreev, J Catal 158 (1996) 354-355.
- [25] D. Andreeva, V. Idakiev, T. Tabakova, A. Andreev, R. Giovanoli, Appl Catal A-Gen 134 (1996) 275-283.
- [26] D. Andreeva, T. Tabakova, V. Idakiev, P. Christov, R. Giovanoli, App Catal A-Gen 169 (1998) 9-14.
- [27] B. Aeijelts Averink Silberova, G. Mul, M. Makkee, J.A. Moulijn, J Catal 243 (2006) 171-182.
- [28] B.A. Silberova, M. Makkee, J.A. Moulijn, Top Catal 44 (2007) 209-221.

- [29] A. Karpenko, Y. Denkwitz, V. Plzak, J. Cai, R. Leppelt, B. Schumacher, R.J. Behm, *Catal Lett* 116 (2007) 105-115.
- [30] H. Daly, A. Goguet, C. Hardacre, F.C. Meunier, R. Pilasombat, D. Thompson, *J Catal* 273 (2010) 257-265.
- [31] K. Li, M. Haneda, Z. Gu, H. Wang, M. Ozawa, *Mater Lett* 93 (2013) 129-132.
- [32] Y. Sunagawa, K. Yamamoto, H. Takahashi, A. Muramatsu, *Catal Today* 132 (2008) 81-87.
- [33] S. Carabineiro, N. Bogdanchikova, M. Avalos-Borja, A. Petryakov, P. Tavares, J. Figueiredo, *Nano Res* 4 (2011) 180-193.
- [34] S.A.C. Carabineiro, B.F. Machado, R.R. Bacsa, P. Serp, G. Dražić, J.L. Faria, J.L. Figueiredo, *J Catal* 273 (2010) 191-198.
- [35] S.A.C. Carabineiro, A.M.T. Silva, G. Dražić, P.B. Tavares, J.L. Figueiredo, *Catal Today* 154 (2010) 21-30.
- [36] S.A.C. Carabineiro, P. Tavares, J. Figueiredo, *Appl Nanoscience* 2 (2012) 35-46.
- [37] M. Bowker, A. Nuhu, J. Soares, *Catal Today* 122 (2007) 245-247.
- [38] S.A.C. Carabineiro, N. Bogdanchikova, P.B. Tavares, J.L. Figueiredo, *RSC Advances* 2 (2012) 2957-2965.
- [39] S.A.C. Carabineiro, S.S.T. Bastos, J.J.M. Órfão, M.F.R. Pereira, J.J. Delgado, J.L. Figueiredo, *App Catal A-Gen* 381 (2010) 150-160.
- [40] S.S.T. Bastos, S.A.C. Carabineiro, J.J.M. Órfão, M.F.R. Pereira, J.J. Delgado, J.L. Figueiredo, *Catal Today* 180 (2012) 148-154.
- [41] E.G. Rodrigues, S.A.C. Carabineiro, J.J. Delgado, X. Chen, M.F.R. Pereira, J.J.M. Órfão, *J Catal* 285 (2012) 83-91.
- [42] S.A.C. Carabineiro, A.M.T. Silva, G. Dražić, P.B. Tavares, J.L. Figueiredo, *Catal Today* 154 (2010) 293-302.
- [43] V.P. Santos, S.A.C. Carabineiro, P.B. Tavares, M.F.R. Pereira, J.J.M. Órfão, J.L. Figueiredo, *App Catal B- Environ* 99 (2010) 198-205.
- [44] F. Moreau, G.C. Bond, A.O. Taylor, *J Catal* 231 (2005) 105-114.
- [45] M.A. Soria, C. Mateos-Pedrero, A. Guerrero-Ruiz, I. Rodríguez-Ramos, *Int J of Hydrogen Energ* 36 (2011) 15212-15220.
- [46] E.D. Park, J.S. Lee, *J Catal* 186 (1999) 1-11.
- [47] W.S. Epling, G.B. Hoflund, J.F. Weaver, S. Tsubota, M. Haruta, *J. Phys. Chem.* 100 (1996) 9929-9934.
- [48] M. Khoudiakov, M.C. Gupta, S. Deevi, *App Catal A-Gen* 291 (2005) 151-161.
- [49] G.J. Hutchings, M.S. Hall, A.F. Carley, P. Landon, B.E. Solsona, C.J. Kiely, A. Herzing, M. Makkee, J.A. Moulijn, A. Overweg, J.C. Fierro-Gonzalez, J. Guzman, B.C. Gates, *J Catal* 242 (2006) 71-81.
- [50] J. Zieliński, I. Zglinicka, L. Znak, Z. Kaszukur, *App Catal A-Gen* 381 (2010) 191-196.
- [51] W.K. Jozwiak, E. Kaczmarek, T.P. Maniecki, W. Ignaczak, W. Maniukiewicz, *App Catal A-Gen* 326 (2007) 17-27.
- [52] A. Venugopal, J. Aluha, D. Mogano, M.S. Scurrell, *Appl Catal A- Gen* 245 (2003) 149-158.
- [53] A. Venugopal, M.S. Scurrell, *Appl Catal A-Gen* 258 (2004) 241-249.
- [54] H.-Y. Lin, Y.-W. Chen, C. Li, *Thermochimica Acta* 400 (2003) 61-67.
- [55] T. Tabakova, G. Avgouropoulos, J. Papavasiliou, M. Manzoli, F. Boccuzzi, K. Tenchev, F. Vindigni, T. Ioannides, *Appl Catal B-Environ* 101 (2011) 256-265.
- [56] B.E. Solsona, T. Garcia, C. Jones, S.H. Taylor, A.F. Carley, G.J. Hutchings, *Appl Catal A-Gen* 312 (2006) 67-76.

- [57] F. Boccuzzi, A. Chiorino, M. Manzoli, D. Andreeva, T. Tabakova, *J Catal* 188 (1999) 176-185.
- [58] G. Wang, H. Lian, W. Zhang, D. Jiang, T. Wu, *Kinet Catal* 43 (2002) 433-442.
- [59] Z. Hao, L. An, H. Wang, T. Hu, *React Kinet Catal Lett.* 70 (2000) 153-160.
- [60] J.-N. Lin, B.-Z. Wan, *App Catal B- Environ* 41 (2003) 83-95.
- [61] J. Hua, K. Wei, Q. Zheng, X. Lin, *App Catal A-Gen* 259 (2004) 121-130.
- [62] J. Li, Y. Zhan, F. Zhang, X. Lin, Q. Zheng, *Chin J Catal* 29 (2008) 346-350.
- [63] A. Luengnaruemitchai, S. Osuwan, E. Gulari, *Catal Commun* 4 (2003) 215-221.
- [64] W. Deng, C. Carpenter, N. Yi, M. Flytzani-Stephanopoulos, *Top Catal* 44 (2007) 199-208.

Tables

Table 1. Properties and experimental conditions employed during tests with Au/Fe₂O₃ catalysts. The variation of XCO as a function of temperature for these catalysts are shown in Figure 15.

% wt. Au	S _{BET} m ² /g	P (atm)	Space velocity or Q/W	Feed	ref
1	14	1	4000 h ⁻¹	4.88 % CO vapour/gas ratio : 0.7	[25]
2	20		4000 h ⁻¹	4.88 % CO vapour/gas ratio : 0.7	[25]
5	6	1	1499 ml h ⁻¹ g ⁻¹	4.7%CO 35.4%H ₂ O 10.1%CO ₂ 28.5 %H ₂	[This work]
8	257	1	2000 ml h ⁻¹ g ⁻¹	10% CO	[61]
n.a	79	1	10000 h ⁻¹	10%CO inN ₂ trough a vaporizer at 82 °C	[62]
3	79	1	30000 ml h ⁻¹ g ⁻¹	4% CO	[63]
0.7	44	1	11.1 ml s ⁻¹ g ⁻¹	2%CO 10.7%H ₂ O	[64]

Figures

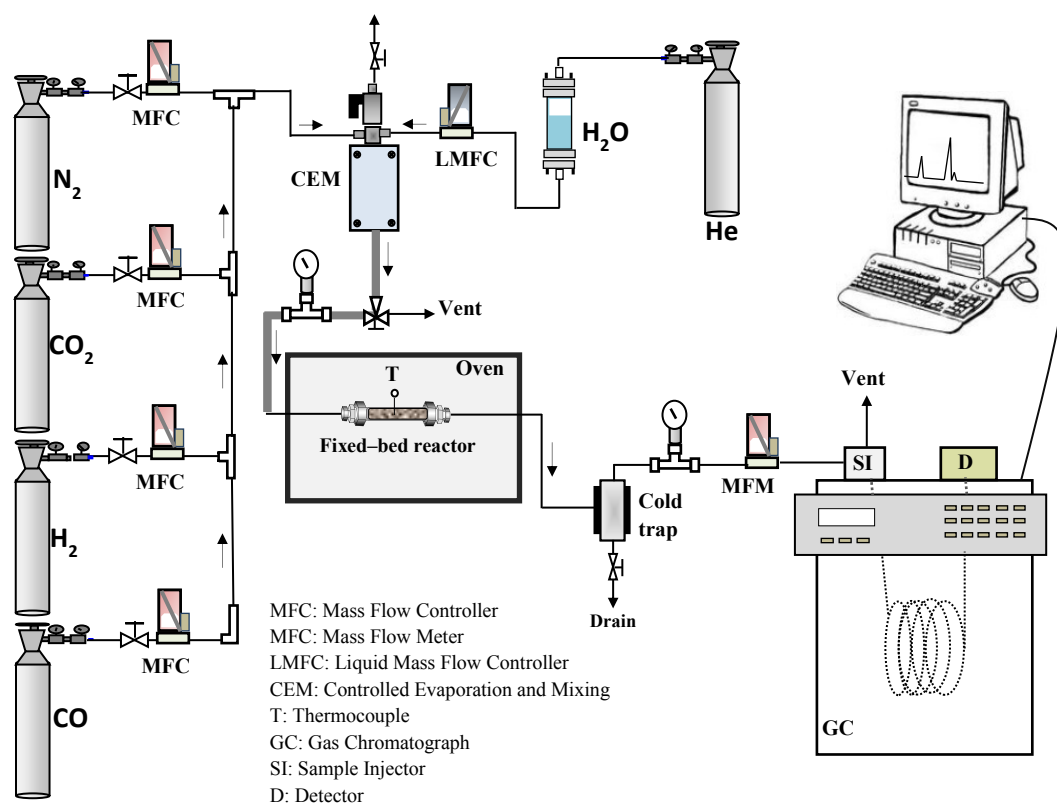


Figure1. Scheme of the set-up used for catalytic activity measurements in the LT-WGS reaction.

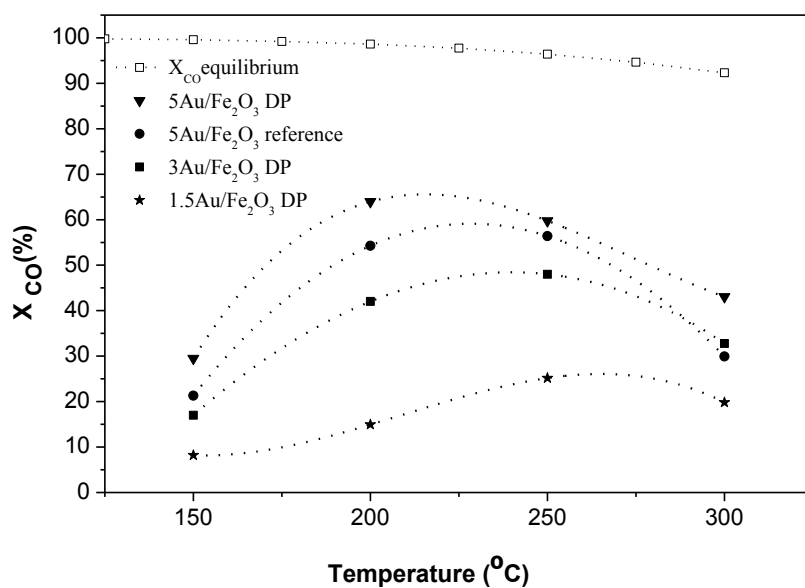


Figure 2. Effect of gold content on CO conversion (X_{CO}) vs. temperature in LT-WGS reaction over Au/Fe₂O₃_DP catalysts; 5Au/Fe₂O₃_reference catalyst is also included. Feed (vol. %): 4.7 CO, 10.1 CO₂, 35.4 H₂O, 28.5 H₂ and 21.3 of N₂. W/Q = 6.67×10^{-5} g h ml_N⁻¹. X_{COeq} = Equilibrium CO conversion at equilibrium.

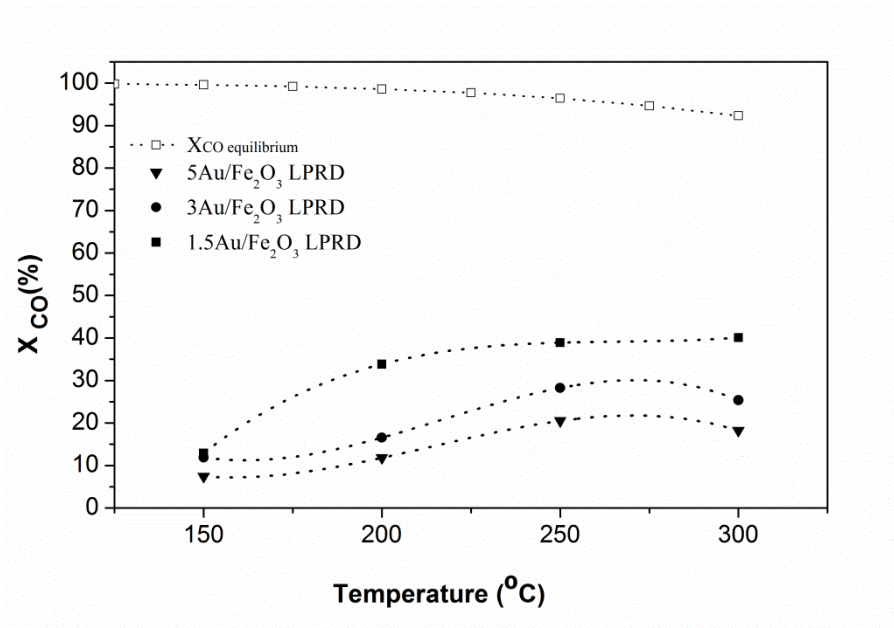


Figure 3. Effect of gold content on CO conversion (X_{CO}) vs. temperature in the LT-WGS reaction over Au/Fe₂O₃_LPRD catalysts. Feed (vol. %): 4.7 CO, 10.1 CO₂, 35.4 H₂O, 28.5 H₂ and 21.3 of N₂. W/Q = 6.67×10^{-5} g h ml_N⁻¹. X_{COeq} = Equilibrium CO conversion at equilibrium.

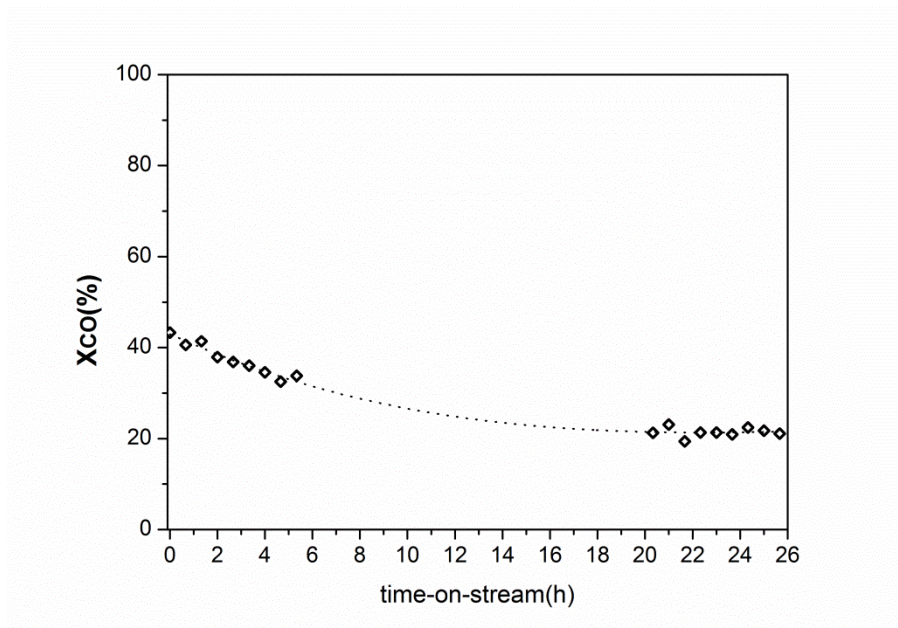


Figure 4. CO conversion history for the 3Au/Fe₂O₃_DP catalyst at 200 °C. Feed (vol. %): 4.7 CO, 10.1 CO₂, 35.4 H₂O, 28.5 H₂ and 21.3 of N₂. W/Q = 6.67×10⁻⁵ g h ml_N⁻¹.

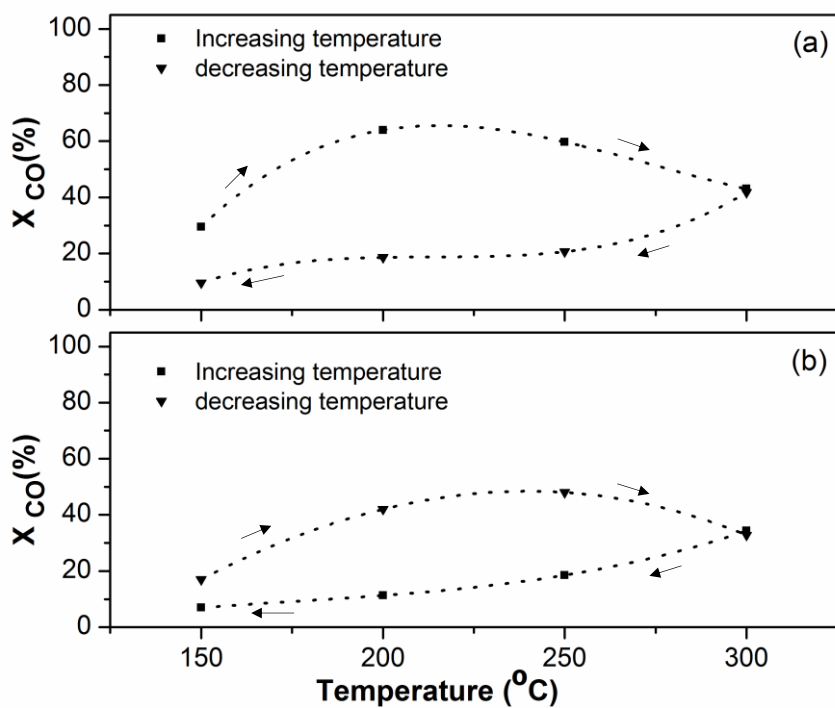


Figure 5. CO conversion (X_{CO}) as a function of temperature in the LT-WGS reaction over the 5Au/Fe₂O₃_DP (a) and 3Au/Fe₂O₃_DP (b) samples; with (■) increasing or (▼) decreasing the reaction temperature. Feed (vol. %): 4.7 CO, 10.1 CO₂, 35.4 H₂O, 28.5 H₂ and 21.3 of N₂. W/Q = 6.67×10^{-5} g h ml_N⁻¹.

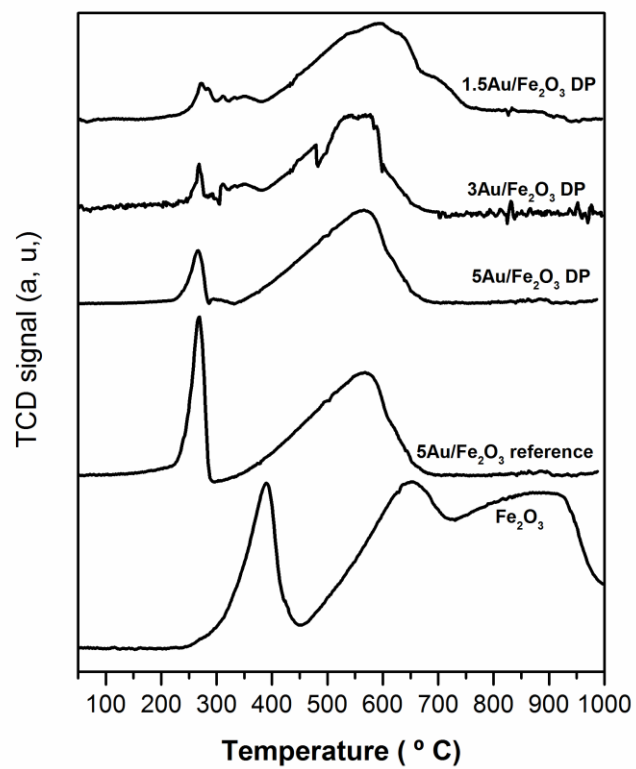


Figure 6. TPR-H₂ profiles of α -Fe₂O₃, 5Au/Fe₂O₃_reference and Au/Fe₂O₃_DP catalysts with different gold contents.

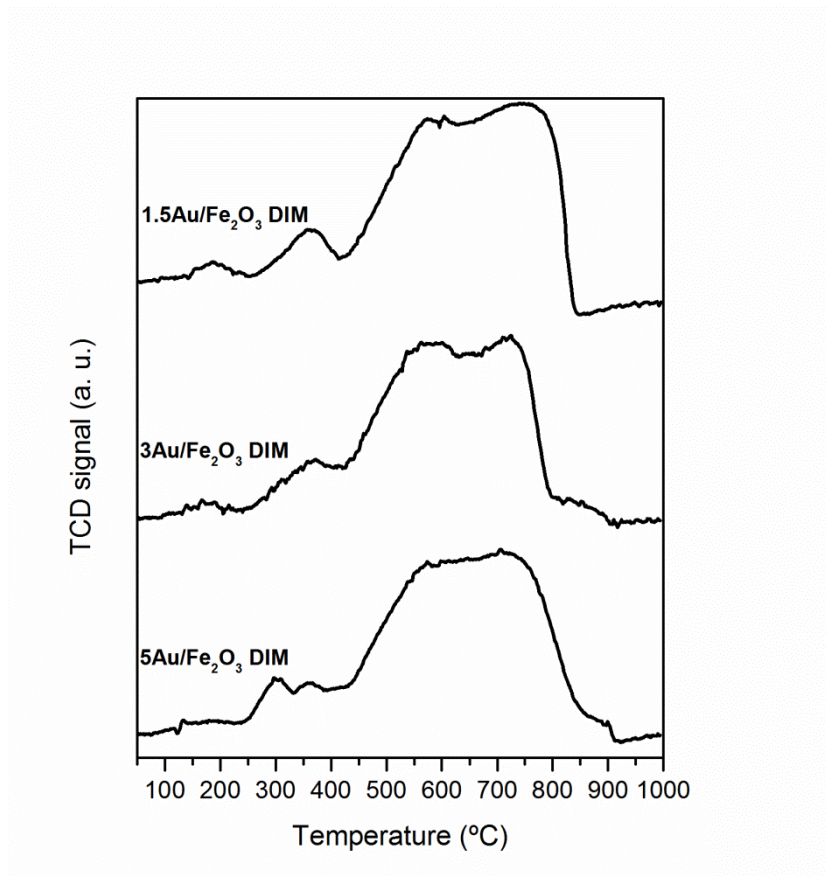


Figure 7. TPR-H₂ profile of Au/Fe₂O₃_DIM catalysts with different gold contents.

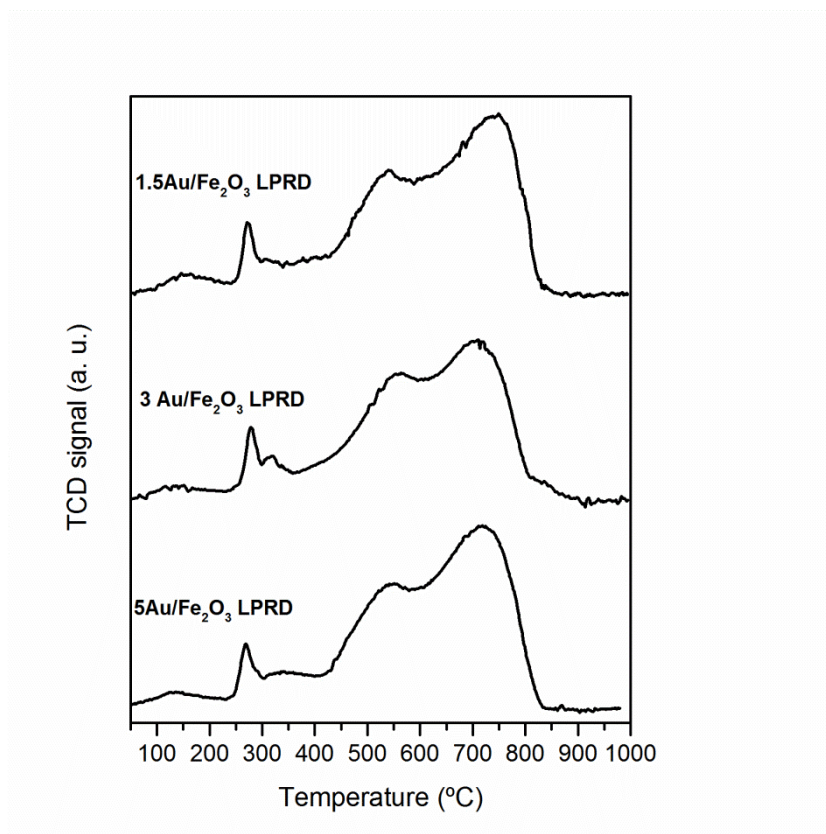


Figure 8. TPR-H₂ profiles of Au/Fe₂O₃_LPRD catalysts with different gold contents.

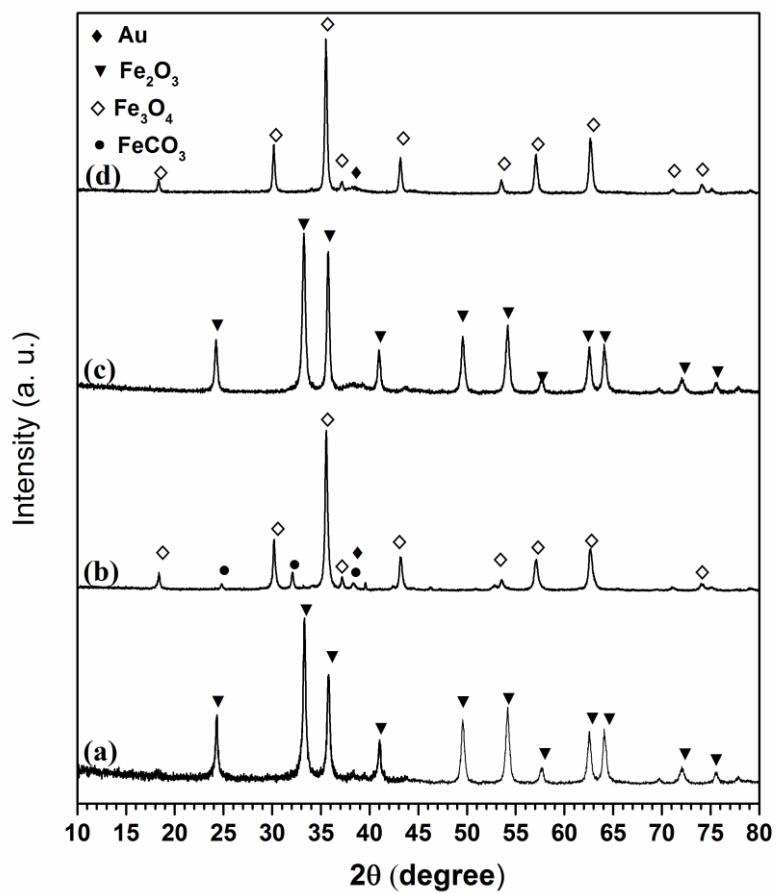


Figure 9. X-ray diffractograms of: (a) $1.5\text{Au}/\text{Fe}_2\text{O}_3\text{-LPRD}$ fresh (b) $1.5\text{Au}/\text{Fe}_2\text{O}_3\text{-LPRD}$ used (c) $5\text{Au}/\text{Fe}_2\text{O}_3\text{-DP}$ fresh and (d) $5\text{Au}/\text{Fe}_2\text{O}_3\text{-DP}$ used catalysts.

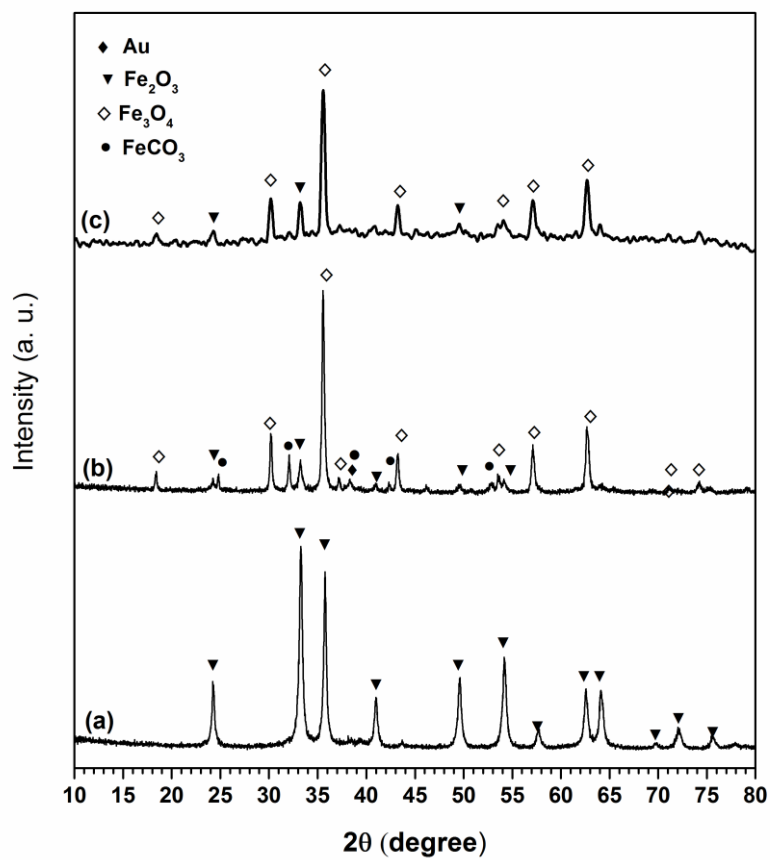


Figure 10. X-ray diffractograms of: (a) 3Au/Fe₂O₃_DP fresh (b) 3Au/Fe₂O₃_DP used and (c) 3Au/Fe₂O₃_DP after stability test (200 °C, 25 h) catalysts.

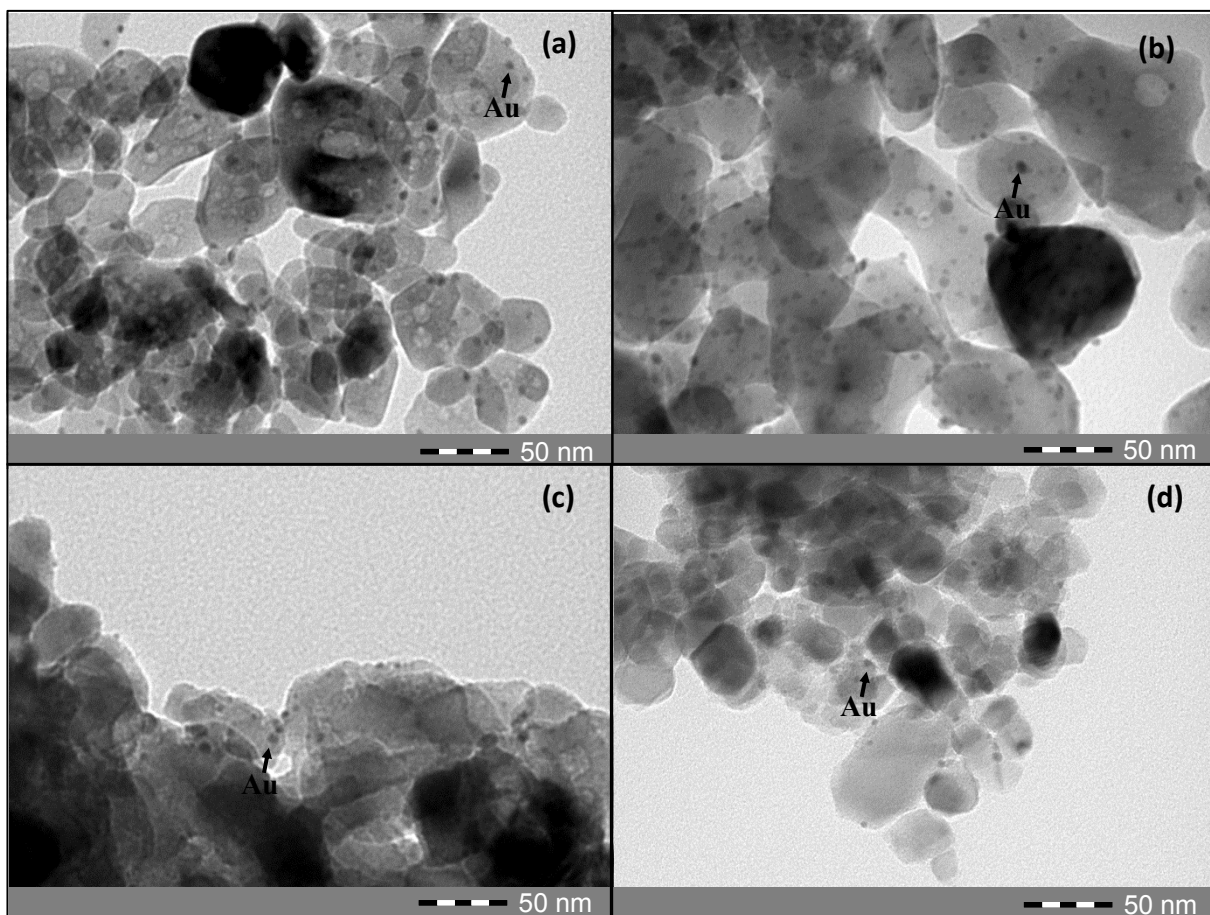


Figure 11. HRTEM images of the (a) 5Au/Fe₂O₃_DP fresh (b) 5Au/Fe₂O₃_DP used (c) 1.5Au/Fe₂O₃_LPRD fresh and (d) 1.5Au/Fe₂O₃_LPRD used.

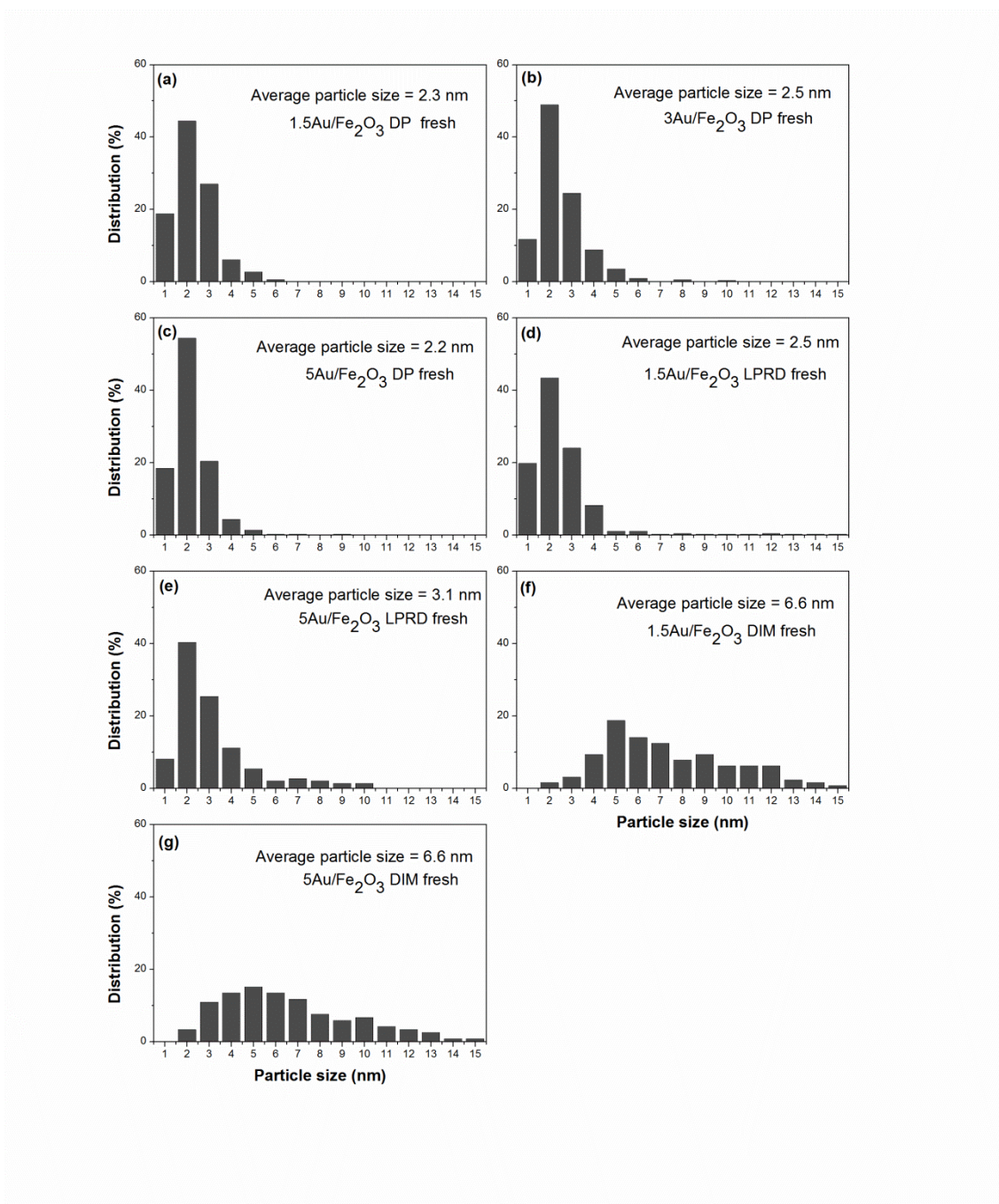


Figure 12. Gold particles size distribution in some fresh catalysts: (a) 1.5Au/Fe₂O₃_DP, (b) 3Au/Fe₂O₃_DP, (c) 5Au/Fe₂O₃_DP, (d) 1.5Au/Fe₂O₃_LPRD, (e) 5Au/Fe₂O₃_LPRD, (f) 1.5Au/Fe₂O₃_DIM and (g) 5Au/Fe₂O₃_DIM.

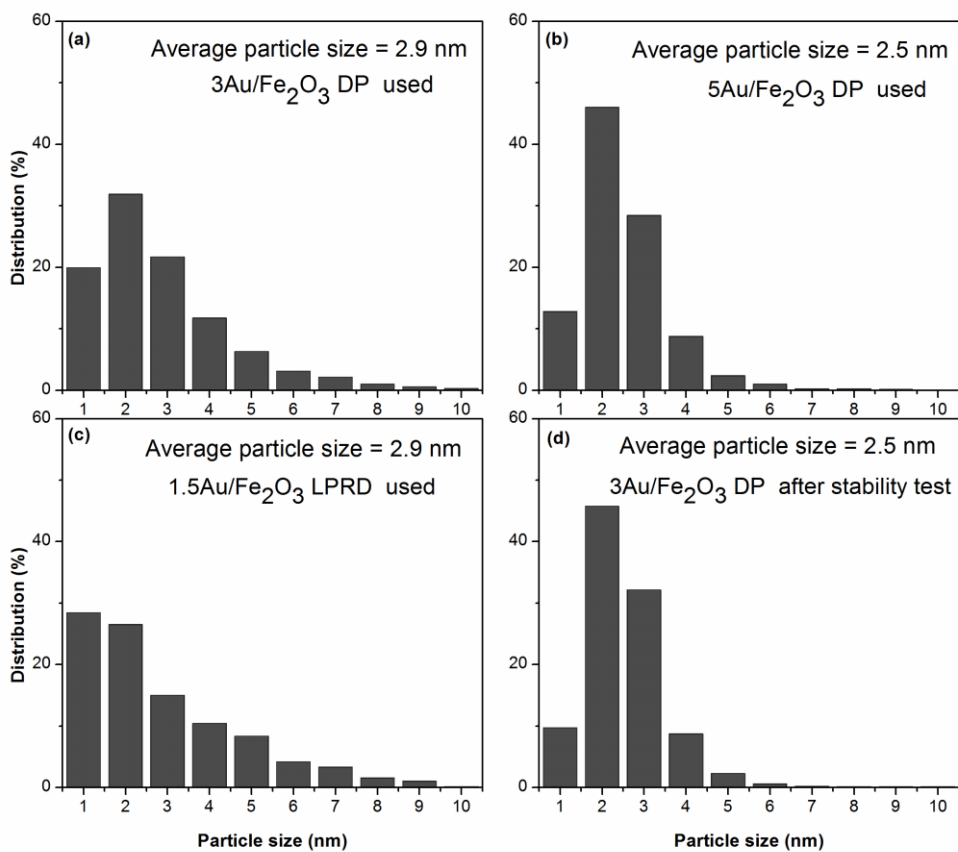


Figure 13. Gold particles size distribution in some used catalysts: (a) 3Au/Fe₂O₃_DP, (b) 5Au/Fe₂O₃_DP and (c) 5Au/Fe₂O₃_LPRD, and (d) 3Au/Fe₂O₃_DP after stability test (200°C, 25h).

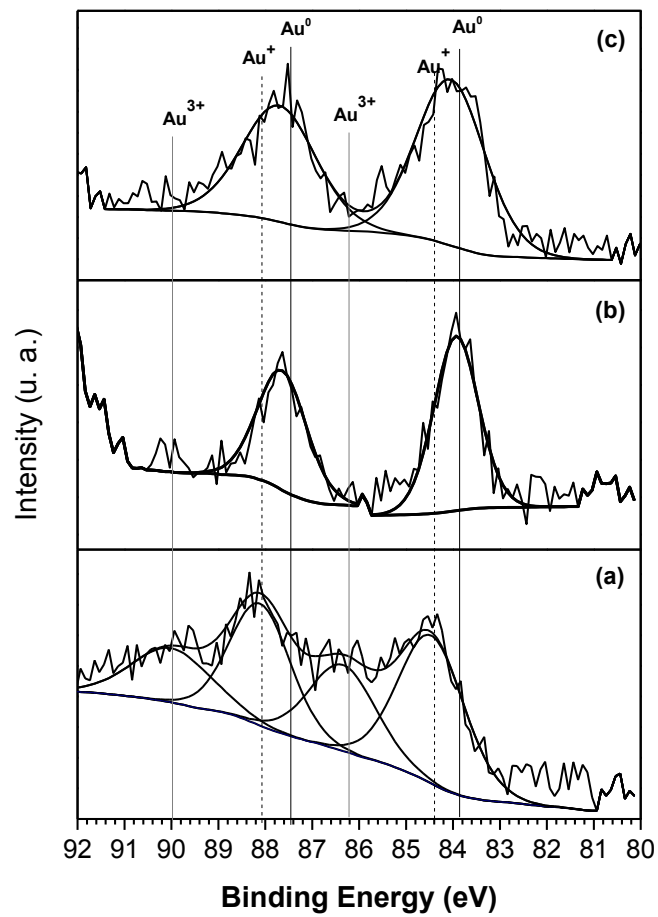


Figure 14. Au 4f XPS spectra of (a) 3Au/Fe₂O₃_DP, (b) 5Au/Fe₂O₃_DIM and (c) 1.5Au/Fe₂O₃_LPRD catalysts.

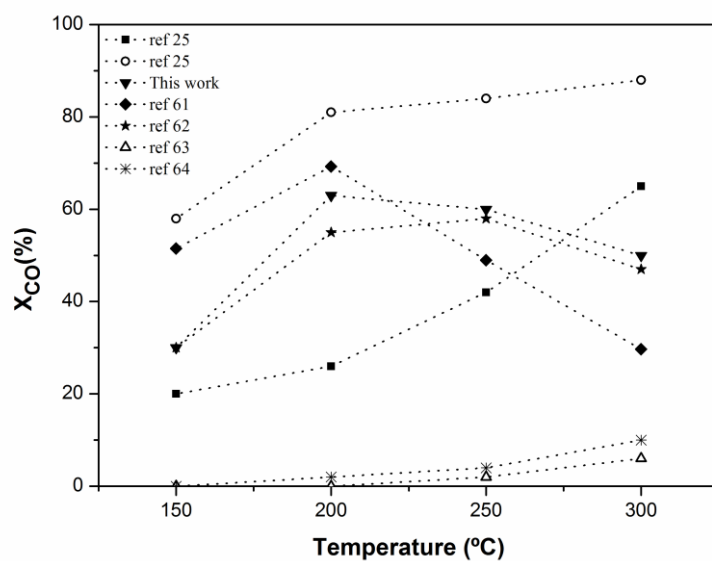


Figure 15. Carbon monoxide conversion vs. temperature for 5Au/Fe₂O₃_DP and other catalysts reported in the literature (experimental conditions and details given in Table 1).